Electronic structure and magnetic properties of $Fe_{0.125}Sn_{0.875}O_2$

Shu-jun Hu,* Shi-shen Yan, Xin-xin Yao, Yan-xue Chen, Guo-lei Liu, and Liang-mo Mei
School of Physics and Microelectronics, Shandong University, Jinan, Shandong, 250100, China
and State Key Laboratory of Crystal Materials, Shandong University, Jinan, 250100, China
(Received 21 November 2006; revised manuscript received 23 January 2007; published 12 March 2007)

The electronic structure of Fe-doped SnO_2 is systematically investigated by means of first-principles calculations. A ferrimagnetic exchange interaction between the dopants, which is rarely found in dilute magnetic semiconductors, is predicted for the ground doping configuration in which two Fe ions are adjacently substituting the Sn sites in a distorted rutile structure. Spin density results reveal the direct exchange interaction between O 2*p* and Fe 3*d* electrons with antiparallel spins, which leads to competition between ferromagnetic and antiferromagnetic superexchange interactions since the doping ions tend to form a special 120° Fe–O–Fe bond. Therefore, a negligible energy difference between the parallel and antiparallel spin alignments is predicted for the ground-state configuration. Moreover, the calculated density of states with both parallel and antiparallel spins shows the nearly 100% spin-polarized states at the Fermi level. An interesting half-metallic antiferromagnetic state reported recently has been also obtained in one of the calculated doping configurations.

DOI: 10.1103/PhysRevB.75.094412 PACS number(s): 75.50.Pp, 75.30.Hx, 75.50.Gg

I. INTRODUCTION

Dilute magnetic semiconductors (DMS's) have attracted much attention because of their promising applications in spintronics.[1,2] Recent experimental reports indicated that the DMS's with high Curie temperature are mainly concentrated in the semiconducting oxides—e.g., ZnO, TiO_2, and SnO_2. Tin dioxide (SnO_2) with a wide band gap is an important semiconductor and has wide applications in many fields. Due to the good stability in high-temperature and environment-dependent surface properties, it has been used as gas sensors, solar cells, and optically transparent materials. Recent researches on realizing room-temperature ferromagnetism in transition-metal-doped SnO_2 (Refs. 3–16) have motivated the experimenters to study the structural, optical, electronic, and magnetic properties, especially the new concept of "giant magnetic moments."[17] Punnoose and co-workers have reported the ferromagnetism of Fe-doped SnO_2 with a Curie temperature $T_c = 850$ K and presented an alternative gas-sensing technology by utilizing this kind of material.[4–7] Moreover, Mössbauer spectra[8,9] indicated that only 23% of the iron atoms order ferromagnetically in the $Sn_{1-x}Fe_xO_2$ transparent magnetic semiconductor where the origin of the ferromagnetic coupling is attributed to the *F* center. For $Sn_{1-x}Co_xO_2$ samples room-temperature ferromagnetism has been only detected in the low doping concentration of $x \leq 0.01$.[10–12] In addition, a giant magnetic moment has also been detected in Cr-doped SnO_2 films[13] besides the $Co_xSn_{1-x}O_{2-\delta}$ samples.[17]

Beyond the discrete data in these reports, it was found that both the crystalline structure and magnetism are sensitive to the doping concentration in most cases. In Refs. 4 and 7 many efforts have been made to study the changes of the lattice parameters and magnetism as a function of Fe doping concentration, suggesting a strong structural-magnetic properties relationship. The variation of the lattice constant in Co-doped samples also reveals the subtle relationship between the structure and magnetism.[11] Additionally Hong *et al.* have prepared Ni-doped SnO_2 thin films on various kinds of substrates and then indicated that the ferromagnetism would be enormously reduced when the constraints on the film were relaxed.[14] Therefore the complex magnetism in various situations may be attributed to the tiny difference of the crystalline structures.

Interestingly, Fe has been considered to be a promising doping source among the transition metal elements. In Ref. 15 the authors indicated that Fe-doped SnO_2 samples exhibit ferromagnetic behavior while Cr-doped SnO_2 films are paramagnetic at 300 K and 5 K. The ferromagnetic moment per Fe atom for $Sn_{0.95}Fe_{0.05}O_2$ samples is much larger than that of Mn-doped samples at room temperature, while only paramagnetism has been detected in Co-doped samples.[9] Recently a systematic experimental investigation was carried out to study the magnetism of transition-metal-doped SnO_2.[16] It was found that Cr-, Mn-, Fe-, Co-, or Ni-doped SnO_2 films are all ferromagnetic at room temperature, but the Fe-doped one has the largest magnetic moment.

To date, only a small amount of theoretical research has been devoted to the electronic structure of transition-metal-doped SnO_2-based ferromagnetic semiconductors, which is essential to understand the origin of ferromagnetism. Computational researches of SnO_2 system are mainly limited to the electronic structure of the bulk,[18] surface,[19] and nonmagnetic-metal-doped systems.[20,21] Based on the experimental attention given to the Fe-doped SnO_2 DMS's, a first-principles computational investigation was undertaken to study the electronic structure of $Fe_{0.125}Sn_{0.875}O_2$ in this paper. The most energetically favorable substituted configuration, the electronic structure of the doped systems, and the magnetic exchange interaction between the dopants are the main questions addressed in this work. Ferrimagnetic spin alignment[22] between the dopants is predicted for the ground substitutional configuration. A universal half-metallic state in the energetically favorable substituting configurations makes this DMS promising in spintronic applications.

II. INVESTIGATED SYSTEMS AND CALCULATION DETAILS

Similar to the well-known TiO_2, SnO_2 bulk has a tetragonal symmetry in rutile structure. The rutile phase is charac-

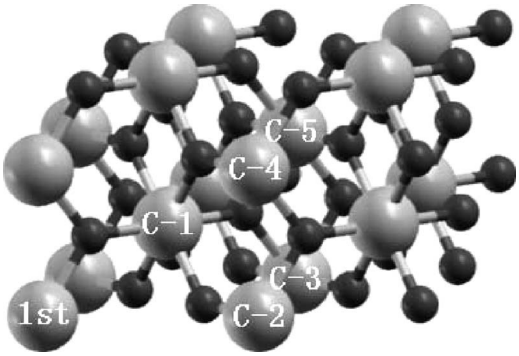

FIG. 1. Side view of the schematic tin dioxide supercell consisting of 16 Sn atoms and 32 O atoms. The large gray balls are Sn and the small dark balls are O.

terized by two lattice parameters a and c and internal parameter u associated with the O atomic position. Using the integer multiples representation of the primitive lattice vectors a_1, a_2, and a_3 of the conventional SnO_2 cell, the geometry of an undoped $2\times2\times2$ supercell containing 48 atoms ($Sn_{16}O_{32}$) is shown in Fig. 1. Considering two Sn sites replaced by Fe atoms and the symmetry of periodic lattice, five different doping configurations are selected in a $Sn_{14}Fe_2O_{32}$ supercell with Fe concentration of 12.5%.[23] In these configurations the second substituted Sn site is marked by C-1–C-5, respectively, besides the first substituted Sn site marked "1st." In C-1, two Fe atoms cluster around the middle O ion—namely, Fe_I-O-Fe_{II}—while in the other four configurations, two Fe atoms are separated within the Fe-O-Sn-O-Fe configuration along different directions.

The total energy calculation and geometry optimizations were performed by using a plane-wave basis set and ultrasoft pseudopotentials[24] in PW91 format,[25] as implemented in the QUANTUM-ESPRESSO package.[26] Brillouin zone integrations were performed by using $4\times4\times4$ Monkhorst and Pack special point grids[27,28] and Methfessel and Paxton smearing technique with a smearing width of 0.005 Ry.[29] The wave functions were expanded in plane waves up to a cutoff energy of 40 Ry for the charge density. The experimental parameters[13] of SnO_2 were first implemented to construct the initial coordinates of a 48-atom $2\times2\times2$ supercell. Structure optimization was then performed in a variable-cell model to obtain the structure parameters in the ground state for the substitutional configurations. As suggested in Ref. 18, the inclusion of gradient corrections for exchange correlation leads to the result that lattice parameter a is greater than experimental value by $\sim3\%$ whereas the c/a ratio and the u parameter are almost unaffected. The force convergence threshold for the atomic relaxation is 10^{-3} Ry/bohr. All the calculations are performed by keeping the volume of doping configurations fixed at the equilibrium volume of the pure $Sn_{16}O_{32}$ cell since the variation of the lattice parameters is small.[7]

III. CALCULATION RESULTS

A. Total energy and magnetism

The ground state was identified by means of calculating the total energy of the supercell with different doping configurations. The energy difference between parallel ($\uparrow\uparrow$) and antiparallel ($\uparrow\downarrow$) spin alignments for each configuration is also calculated to give a general estimation of the Curie temperature. The relative energies of parallel and antiparallel states for the other configurations with respect of that of the ground state are listed in Table I. Calculation results show that the adjacently substitutional configuration—i.e., C-1 in $\uparrow\downarrow$ spin alignment—is energetically favorable. The magnetic moment per supercell for all configurations is also given in Table I. For configurations C-2–C-5, the energy difference between $\uparrow\uparrow$ and $\uparrow\downarrow$ spin alignments is relatively small whereas the total energy is much higher than that of the ground state, indicating a clustering trend of the dopants in the SnO_2 matrix. The clustering trend has been experimentally verified to be common by the inhomogeneous analysis of the prepared DMS samples.[30–32] In Ref. 8 energy-dispersive x-ray diffraction spectroscopy indicated the nonuniform iron distribution in the $Fe_xSn_{1-x}O_2$ source targets, which directly supports our theoretical results.

Interestingly, C-1 in $\uparrow\downarrow$ spin alignment owns a net magnetic moment of $2\mu_B$ (average $1\mu_B$ per Fe ion) rather than zero. Consequently, it is expected that this material will behave like ferrimagnets with antiparallel and small net moments. The relatively small net moment of Fe atoms is in good agreement with the experimental results.[9] It is worthy to mention that the ferrimagnetic coupling is rarely found in the *collinear* magnetism calculations of DMS's.[33] That is why we call it "antiparallel spin alignment" rather than "antiferromagnetic spin alignment" in this candidate. It was found that the small net moment accompanied by the ferrimagnetic coupling originates from the lattice distortion of the relaxed supercell which will be discussed in detail combined with the band structure in the following. Although C-1 in $\uparrow\downarrow$ spin alignment is energetically favorable, the energy difference between the $\uparrow\uparrow$ and $\uparrow\downarrow$ spin alignments is small—only about 6 meV. Considering such small energy difference, partial doping ions in the prepared metastable samples may be ordered magnetically, which is in agreement with the experimental results.[8]

B. Band structure of C-1

Figure 2 shows the calculated density of states (DOS) of C-1 and Fe $3d$ projected components on the Fe sites, respectively. For the purpose of comparison, a $Sn_{16}O_{32}$ supercell representing the host material and a $FeSn_{15}O_{32}$ system named C-0 in which only one Sn atom is substituted by Fe ions were also studied, which are shown in Figs. 3(a) and 3(b), respectively. The zero of the energy is set at the Fermi level. As shown in Fig. 3(a) the calculated band gap of the host SnO_2 is much smaller than the experimental value due to the band gap underestimation of the local density approximation (LDA). In the case of $FeSn_{15}O_{32}$ [Fig. 3(b)] the Fe $3d$ orbital is split into triple states with lower energy and double states with higher energy by the *octahedral-like* crystal field in C-0. The effect of exchange splitting is larger than that of the crystal field and results in a nearly single-spin state near the Fermi level, which is in agreement with the previous theoretical prediction.[34] There are few changes for the DOS

TABLE I. The calculated total magnetization and energy difference between parallel and antiparallel spin alignments of the doping configurations C-0–C-5. The last column shows the energy difference of various configurations compared with the ground state—i.e., C-1 in antiparallel spin alignment.

Configuration	Spin arrangement	Magnetic moment (μ_B/supercell)	Ground state and $\Delta E_{\text{FM-AFM}}$ (meV)	Energy difference relative to C-1 in ↑↓ (meV)
C-0		4.00		
C-1	↑↓	2.00	AFM +5.56	Ground configuration
	↑↑	8.00		5.56
C-2	↑↓	0.04	FM −44.35	319.21
	↑↑	8.00		274.87
C-3	↑↓	0.00	FM −74.39	327.05
	↑↑	8.00		252.65
C-4	↑↓	0.00	FM −25.85	134.17
	↑↑	8.00		108.32
C-5	↑↓	0.00	AFM +56.97	243.68
	↑↑	8.00		300.66

of C-1 in ↑↑ spin alignment compared with $FeSn_{15}O_{32}$. However, the DOS of C-1 in ↑↓ spin alignment is very strange where the majority and minority spins are *no longer symmetrical* as in the usual antiferromagnetic DMS's, as shown in Fig. 2. Additionally the DOS of both spin alignments are very similar and near the Fermi level both are nearly 100% spin polarized. It is found that a half-metallic or near-half-metallic state is common in the several energetically favorable substitutional configurations—i.e., both the parallel and antiparallel spin alignments of C-1 and C-3 and the parallel spin alignment of C-2, C-4, and C-5 (not given in the figure). Here it should be noticed that the half-metallic DOS at the

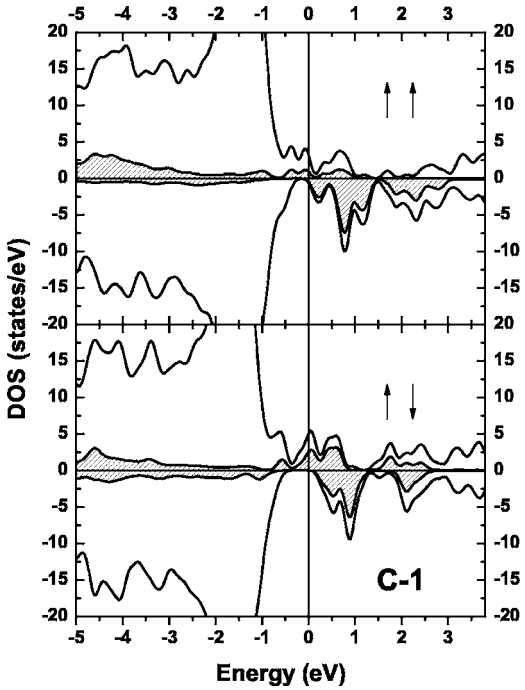

FIG. 2. Total and Fe 3*d* projected DOS of C-1. Upper panel shows the results of parallel spin alignment and lower for the antiparallel spin alignment. The shaded area represents the Fe 3*d* states.

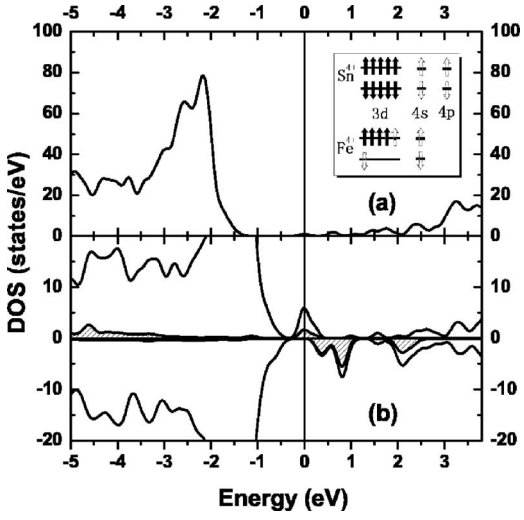

FIG. 3. (a) The total DOS of the $Sn_{16}O_{32}$ supercell. Here a spin-restricted calculation was performed since the SnO_2 host is a nonmagnetic semiconductor. (b) The total and Fe 3*d* projected DOS of C-0. The shaded area shows the Fe 3*d* states. For the majority spin, the triple states are fully occupied while the double states are partially occupied, since the Fe^{2+} cations tend to lose an additional two 3*d* electrons to compensate the effect of substituting one Sn^{4+} ion. (Inset: the valence electron schemes of Sn^{4+} and the doped Fe^{4+} ion.)

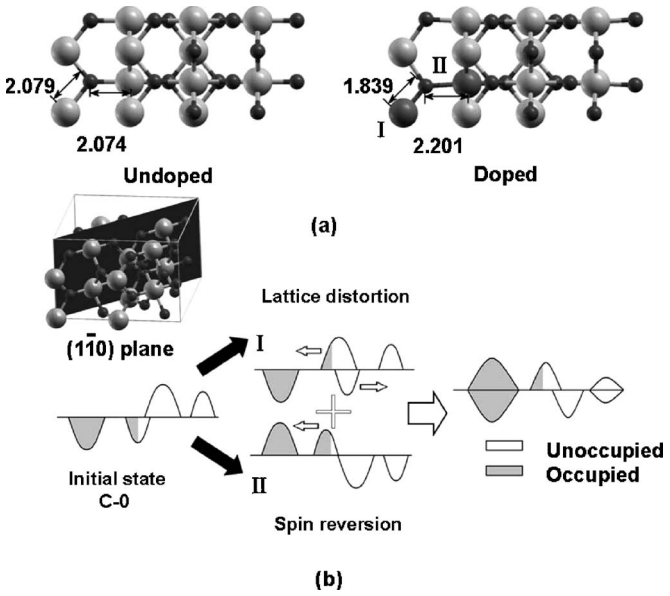

FIG. 4. Lattice-distortion-induced ferrimagnetic exchange interaction between the dopants in the shaded (1$\bar{1}$0) plane. Larger dark balls represent the substitutional Fe ions and are marked by I and II, respectively. Upper panel shows the (a) variation of relaxed crystal structure by doping Fe ions and lower panel for the (b) schematic view of the distorted band structures of C-0 and C-1. The Fe-O distances are in Å, and the precision of the calculated bond-length is about 10^{-3} Å. (The force convergence threshold for the atomic relaxation and the relaxation time step are 10^{-3} Ry/bohr and 2 fs, respectively.) Note that the projected DOS of Fe 3*d* electrons in C-0 is reversed compared with Fig. 3 to conveniently give a schematic view of the results of C-1.

Fermi level is mainly derived from the O 2*p* states and only less than half of the total states were contributed by Fe 3*d* states. Such strong $p-d$ hybridization is rarely found earlier when the 3*d* electrons form an impurity band in the gap, which is essential to mediate the exchange interactions between the doped transition metal ions.

By inspecting the relaxed structure it was found that the ferrimagnetic coupling originates from the lattice distortion of Fe_I-O-Fe_{II}. Figure 4 gives the crystal structure and a schematic view of the DOS with and without the distortion of C-1 in $\uparrow\downarrow$ spin alignment and C-0, respectively. The Fe_I–O bond is significantly reduced while the O–Fe_{II} bond is slightly elongated. Such distortion is expected to originate from the strong *p-d* hybridization and the smaller substitutional ion radius compared with the Sn^{4+}. The Fe–O bond length in NiAs phase FeO (Ref. 35) is slightly larger than that of the Sn–O bond in rutile structure. In addition, the constraint along the O–Fe_{II} bond is smaller than that in the perpendicular plane. Therefore the O–Fe_{II} bond can be freely elongated, which significantly distorts the crystal structure around the middle O ion. Such distortion may be verified by an extended x-ray absorption fine structure (EXAFS) measurement which has been applied in the investigation of Co-doped TiO_2.[36] Interestingly the lattice reconstruction in Fe-doped SnO_2 is very similar to the case of transition-metal-doped rutile TiO_2.[37,38] Although for the host matrix the Ti–O bond length is slightly smaller than that of Sn–O bond, the

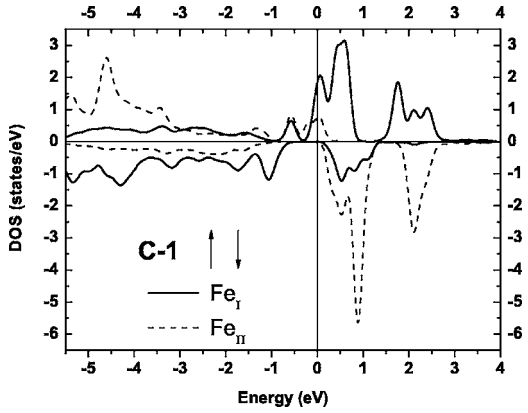

FIG. 5. Fe 3*d* projected DOS of C-1. The solid line represents the contribution of Fe_I and the dashed line for Fe_{II}.

doped crystal structures of both candidates are similar, especially for the case of Cu-doped TiO_2 in Ref. 38. The crystal distortion induces the asymmetry of majority and minority spins when the magnetic moments are antiparallel aligned. There is no obvious change for the DOS of the Fe_{II} ion (see Fig. 5 for the Fe 3*d* projected DOS) except the slight depression of the spin-up double states. However, the spin-down double states are significantly pushed to higher energies by the closer O ion in the Fe_I–O bond and the energy of spin-up triple states are depressed due to the local exchange interaction. Therefore the ferrimagnetic coupling between two dopants results in 100% spin polarization at the Fermi level.

C. Spin density of C-0 and C-1

Here we discuss the origin of ferrimagnetism in terms of spin density and 120° superexchange between O anions and Fe cations. The charge density is generally utilized to represent the formation of a covalent bond and the interaction between the ions. However, it is faint for revealing the origin of the ferromagnetism, especially the exchange interaction in magnetic materials since the dense charge screens the spin polarization. Figure 6 shows the spin density of C-0 and C-1 in different spin alignments, which directly reveals the $\uparrow\downarrow$ coupling between the 3*d* and 2*p* electrons attributed to the cation and anion, respectively. SnO_2 has a rutile structure in which three bonds formed by O 2*p* electrons are coplanar around the O site with the 120° cation-O-cation angle. In Fig. 6(a) six O anions [four presented in the shaded (1$\bar{1}$0) plane] in FeO_6 ligand are polarized with the major polarized elements along the Fe–O bond in C-0. Similarly the O anion between the dopants is significantly polarized in C-1 as shown in Figs. 6(b) and 6(c). Obviously, the slight difference of spin between the $\uparrow\uparrow$ and $\uparrow\downarrow$ spin alignments shows that (i) the Fe 3*d* electrons tend to interact with the neighboring O 2*p* electrons of opposite spin to their own and (ii) the distribution of polarized component is mainly parallel or perpendicular to the Fe_I–O bond. Theoretical predictions of antiferromagnetic coupling between transition metal cations and anions was reported in the early literature.[39] It was considered to be an important part of the indirect superexchange mechanism[40] in DMS's. In Fig. 6(b), Fe_I 3*d* and O 2*p* elec-

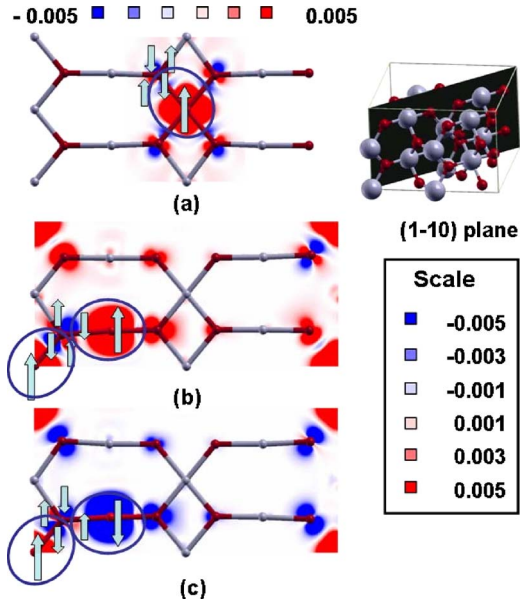

FIG. 6. (Color online) Spin density of (a) C-0 and C-1 in (b) parallel and (c) antiparallel spin alignments in the $(1\bar{1}0)$ plane shows the exchange interactions between O $2p$ and Fe $3d$ ions. The O ligand around or between the dopants is visibly polarized. Blue circles show the area of $\uparrow\downarrow$ direct exchange occurring between O $2p$ and Fe $3d$ electrons and gray arrows indicate the spin orientation.

trons are antiferromagnetically coupled along the Fe_I–O bond. However, considering the magnetic moment ordering there is much difference between the Fe_I–O and O–Fe_{II} bonds. The positively and negatively polarized O $2p$ electrons are on the equal footing to participate in forming the O–Fe_{II} bond [see also Fig. 6(c)] and Fe_{II} $3d$ electrons tend to be coupled with the opposite spin component from the anion. Finally the competition between ferromagnetic superexchange (180° Fe_I-O-Fe_{II}) and antiferromagnetic superexchange (90° Fe_I-O-Fe_{II}), which is opposite to the mechanism revealed in Refs. 22 and 41, leads to the small energy difference between $\uparrow\downarrow$ and $\uparrow\uparrow$ spin alignments.

IV. FURTHER DISCUSSION

First we would like to discuss the reliability of the calculated results. Profiting from the increasing of the computation capabilities, much effort now has been taken to check the computational parameters, selected supercells, and even the reliability of the program code besides the main work in order to obtain more accurate results. In a recent report[22] of an *ab initio* study of transition-metal-doped ZnO, the authors indicated that the calculated magnetic ground state is sensitive to the k-point mesh, energy cutoff, and even the choice of the exchange-correlation functional. By checking the reliability of the computational parameters in this work, it was found that taking C-1 in antiparallel spin alignment as example, the total energy $E_{\uparrow\downarrow}$ would be changed from −3815.511 011 Ry to −3815.511 078 Ry when decreasing the force convergence threshold from 10^{-3} Ry/bohr to 10^{-4} Ry/bohr. Therefore the prediction of the magnetic ground state is not sensitive to the stricter value. Although the increase of the kinetic cutoff energy from 40 Ry to 60 Ry can slightly decrease the total energy, it has little influence on the energy difference between the configurations in $\uparrow\uparrow$ and $\uparrow\downarrow$ spin alignments. Additionally it was found that by using the PBE-type pseudopotentials[42] the calculated magnetic moment is the same as the results by using PW91 type. Much denser k-point meshes of $6\times6\times6$ also made no essential improvement in the total energy. Therefore it is believed that the calculation results are robust and the ferrimagnetism is intrinsic in this candidate if *lattice distortion does exist*.

In Ref. 7 the authors indicated that the prepared Fe-doped SnO_2 samples are under compressive strain. In our extensive investigations, variable-cell calculations have been performed to obtain fully relaxed crystal structures. It was found that the lattice parameter a of the convergent configuration is reduced about 0.4%, which is in good agreement with the experimental data.[7] Moreover, after the full relaxation the ferrimagnetism is completely destroyed without any net moment. Such a result is similar to the case of Ni-doped SnO_2 (Ref. 14) in which (i) the magnetization is sensitive to the constraints of the substrate and (ii) a larger substrate where the doped crystalline is more relaxed depresses the ferromagnetism. Therefore the complex magnetism in various cases would be highly sensitive to the crystalline structure as revealed in this work. However, it should be indicated that the crystal matrix of the as-prepared samples would be fixed at the host structure under dilute and low-temperature preparation conditions. Therefore in our studies all the calculations are performed by fixing the volume of doping configurations at the equilibrium volume of the pure $Sn_{16}O_{32}$ cell for the purpose of simulating the actual crystalline environment of the as-prepared samples.

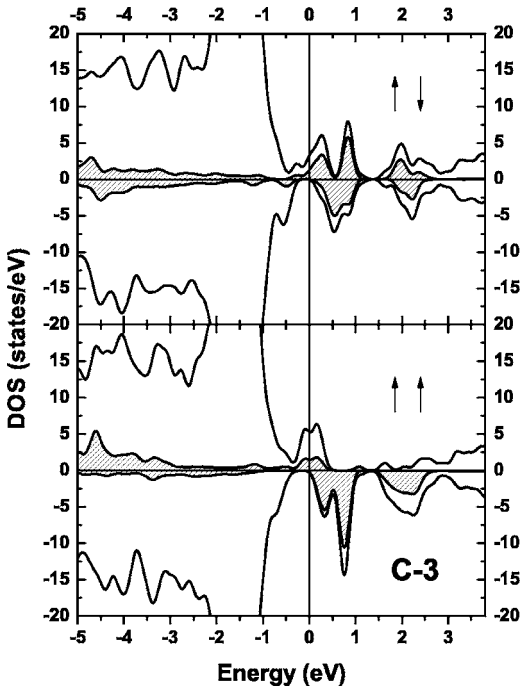

FIG. 7. Total and Fe $3d$ projected DOS of C-3. Upper panel shows the results of parallel spin alignment and lower for the antiparallel spin alignment. The shaded area shows the Fe $3d$ states.

In this work it was found that a half-metallic DOS is common in the several energetically favorable substituting configurations. Half metals, including semi-Heusler alloys,[43] manganese perovskites,[44] chromium dioxide,[45] and magnetite,[46] exhibit metallic and insulating behavior for the majority-spin and minority-spin electrons, respectively. Such materials have shown potential applications to spintronics devices. However, Dowben and Skomski[47] indicated that such materials would suffer from fundamental limitations with surfaces, interfaces, and structural inhomogeneities or when used at finite temperatures. In the extensive calculation studies of Cr-doped SnO_2 it was found that the half-metallic DOS is more significant over a range of ~2 eV near the Fermi level for the energetically and magnetically favorable state. Therefore the transition-metal-doped SnO_2 DMS is expected to exhibit robust half-metallic behavior and to be an ideal material for spintronic applications.

Recently, an attractive report suggested the possibility of half-metallic antiferromagnetism in DMS's.[48] The total magnetization vanishes when the magnetic moments form antiferromagnetic spin ordering, whereas a half-metallic electronic structure would be realized. The authors indicated that it needs at least two certain types of magnetic ions to realize a half-metallic electronic structure in which one has less than half filled 3*d* electrons and the other has more than half filled 3*d* electrons. In this work the half-metallic antiferromagnetic DOS has been found in configuration C-3 and is shown in Fig. 7. The majority- and minority-spin states are basically symmetric for C-3 in $\uparrow\downarrow$ spin alignment in the whole energy range except near the Fermi level. However, this configuration is not energetically favorable and the origin of such DOS is ambiguous. Nevertheless, considering the larger lattice distortion, it is predicted that *single-type* transition-metal-ion-doped half-metallic antiferromagnetic DMS's may be realized by using SnO_2 as the doping matrix.

V. CONCLUSIONS

In summary we have performed a systematic investigation of $Fe_{0.125}Sn_{0.875}O_2$ DMS's implementing first-principles calculations. Both ferrimagnetic exchange interactions between the dopants and half-metallic state at the Fermi level have been predicted in this potential candidate. Spin density schemes are then applied to reveal the direct exchange between the antiparallel spins of O 2*p* and Fe 3*d* electrons and the competition between 180° ferromagnetic superexchange and 90° antiferromagnetic superexchange. Large lattice distortion in transition-metal-doped SnO_2 is predicted in this work, which is expected to induce the ferrimagnetism and high spin polarization. Based on the above theoretical results, the transition-metal-doped SnO_2 DMS is predicted to be promising in spintronic applications.

ACKNOWLEDGMENTS

This work was supported by NSF Grant No. 50572053 and New Century Fund for Outstanding Scholars (Grant No. 040634).

*Corresponding author. FAX: +86-531-88377032. Electronic address: hushujun@mail.sdu.edu.cn

[1] H. Ohno, Science **281**, 951 (1998).
[2] T. Dietl, H. Ohno, F. Matsukura, J. Cibert, and D. Ferrand, Science **287**, 1019 (2000).
[3] J. M. D. Coey, M. Venkatesan, and C. B. Fitzgerald, Nat. Mater. **4**, 173 (2005).
[4] A. Punnoose, J. Hays, A. Thurber, M. H. Engelhard, R. K. Kukkadapu, C. Wang, V. Shutthanandan, and S. Thevuthasan, Phys. Rev. B **72**, 054402 (2005).
[5] A. Punnoose, K. M. Reddy, J. Hays, A. Thurber, and M. H. Engelhard, Appl. Phys. Lett. **89**, 112509 (2006).
[6] A. Punnoose and J. Hays, J. Appl. Phys. **97**, 10D321 (2005).
[7] X. Mathew, J. P. Enriquez, C. Mejía-García, G. Contreras-Puente, M. A. Cortes-Jacome, J. A. Toledo Antonio, J. Hays, and A. Punnoose, J. Appl. Phys. **100**, 073907 (2006).
[8] J. M. D. Coey, A. P. Douvalis, C. B. Fitzgerald, and M. Venkatesan, Appl. Phys. Lett. **84**, 1332 (2004).
[9] C. B. Fitzgerald, M. Venkatesan, A. P. Douvalis, S. Huber, J. M. D. Coey, and T. Bakas, J. Appl. Phys. **95**, 7390 (2004).
[10] A. Punnoose, J. Hays, V. Gopal, and V. Shutthanandan, Appl. Phys. Lett. **85**, 1559 (2004).
[11] J. Hays, A. Punnoose, R. Baldner, M. H. Engelhard, J. Peloquin, and K. M. Reddy, Phys. Rev. B **72**, 075203 (2005).
[12] S. K. Misra, S. I. Andronenko, K. M. Reddy, J. Hays, and A. Punnoose, J. Appl. Phys. **99**, 08M106 (2006).
[13] N. H. Hong, J. Sakai, W. Prellier, and A. Hassini, J. Phys.: Condens. Matter **17**, 1697 (2005).
[14] N. H. Hong, J. Sakai, N. T. Huong, N. Poirot, and A. Ruyter, Phys. Rev. B **72**, 045336 (2005).
[15] W. Wang, Z. Wang, Y. Hong, J. Tang, and M. Yu, J. Appl. Phys. **99**, 08M115 (2006).
[16] C. B. Fitzgerald, M. Venkatesan, L. S. Dorneles, R. Gunning, P. Stamenov, J. M. D. Coey, P. A. Stampe, R. J. Kennedy, E. C. Moreira, and U. S. Sias, Phys. Rev. B **74**, 115307 (2006).
[17] S. B. Ogale, R. J. Choudhary, J. P. Buban, S. E. Lofland, S. R. Shinde, S. N. Kale, V. N. Kulkarni, J. Higgins, C. Lanci, J. R. Simpson, N. D. Browning, S. Das Sarma, H. D. Drew, R. L. Greene, and T. Venkatesan, Phys. Rev. Lett. **91**, 077205 (2003).
[18] J. Goniakowski, J. M. Holender, L. N. Kantorovich, M. J. Gillan, and J. A. White, Phys. Rev. B **53**, 957 (1996).
[19] T. J. Godin and John P. LaFemina, Phys. Rev. B **47**, 6518 (1993).
[20] K. C. Mishra, K. H. Johnson, and P. C. Schmidt, Phys. Rev. B **51**, 13972 (1995).
[21] W. Lin, Y. Zhang, Y. Li, K. Ding, J. Li, and Y. Xu, J. Chem. Phys. **124**, 054704 (2006).
[22] P. Gopal and N. A. Spaldin, Phys. Rev. B **74**, 094418 (2006).
[23] In fact there are six different configurations in all when considering the symmetry, including the unstudied one where iron atoms align along the *c* axis. This configuration is so singular under the periodic condition that it was abandoned.
[24] D. Vanderbilt, Phys. Rev. B **41**, 7892 (1990).

[25] Y. Wang and J. P. Perdew, Phys. Rev. B **43**, 8911 (1991).
[26] S. Baroni, A. Dal Corso, S. de Gironcoli, P. Giannozzi, C. Cavazzoni, G. Ballabio, S. Scandolo, G. Chiarotti, P. Focher, A. Pasquarello, K. Laasonen, A. Trave, R. Car, N. Marzari, and A. Kokalj, http://www.pwscf.org/.
[27] H. J. Monkhorst and J. D. Pack, Phys. Rev. B **13**, 5188 (1976).
[28] J. D. Pack and H. J. Monkhorst, Phys. Rev. B **16**, 1748 (1977).
[29] M. Methfessel and A. T. Paxton, Phys. Rev. B **40**, 3616 (1989).
[30] M. Jamet, A. Barski, T. Devillers, V. Poydenot, R. Dujardin, P. Bayle-Guillemaud, J. Rothman, E. Bellet-Amalric, A. Marty, J. Cibert, R. Mattana, and S. Tatarenko, Nat. Mater. **5**, 653 (2006).
[31] J.-S. Kang, G. Kim, S. C. Wi, S. S. Lee, S. Choi, Sunglae Cho, S. W. Han, K. H. Kim, H. J. Song, H. J. Shin, A. Sekiyama, S. Kasai, S. Suga, and B. I. Min, Phys. Rev. Lett. **94**, 147202 (2005).
[32] H. Q. Song, L. M. Mei, S. S. Yan, X. L. Ma, J. P. Liu, Y. Wang, and Z. Zhang, J. Appl. Phys. **99**, 123903 (2006).
[33] X. Y. Cui, J. E. Medvedeva, B. Delley, A. J. Freeman, N. Newman, and C. Stampfl, Phys. Rev. Lett. **95**, 256404 (2005).
[34] J. M. D. Coey and S. Sanvito, J. Phys. D **37**, 988 (2004).
[35] W. Ranke, M. Ritter, and W. Weiss, Phys. Rev. B **60**, 1527 (1999).
[36] Y. L. Soo, G. Kioseoglou, S. Kim, Y. H. Kao, P. Sujatha Devi, John Parise, R. J. Gambino, and P. I. Gouma, Appl. Phys. Lett. **81**, 655 (2002).
[37] L. A. Errico, G. Fabricius, M. Rentería, P. de la Presa, and M. Forker, Phys. Rev. Lett. **89**, 055503 (2002).
[38] L. A. Errico, M. Rentería, and M. Weissmann, Phys. Rev. B **72**, 184425 (2005).
[39] X. Huang, A. Makmal, J. R. Chelikowsky, and L. Kronik, Phys. Rev. Lett. **94**, 236801 (2005).
[40] P. W. Anderson, Phys. Rev. **79**, 350 (1950).
[41] R. Janisch and N. A. Spaldin, Phys. Rev. B **73**, 035201 (2006).
[42] J. P. Perdew, K. Burke, and M. Ernzerhof, Phys. Rev. Lett. **77**, 3865 (1996).
[43] R. A. de Groot, F. M. Mueller, P. G. van Engen, and K. H. J. Buschow, Phys. Rev. Lett. **50**, 2024 (1983).
[44] K.-I. Kobayashi, T. Kimura, H. Sawada, K. Terakura, and Y. Tokura, Nature (London) **395**, 677 (1998).
[45] M. A. Korotin, V. I. Anisimov, D. I. Khomskii, and G. A. Sawatzky, Phys. Rev. Lett. **80**, 4305 (1998).
[46] F. Walz, J. Phys.: Condens. Matter **14**, R285 (2002).
[47] P. A. Dowben and R. Skomski, J. Appl. Phys. **95**, 7453 (2004).
[48] H. Akai and M. Ogura, Phys. Rev. Lett. **97**, 026401 (2006).